Quantum Electronics **51** (9) 751–758 (2021)

INTERACTION OF EXTREME LIGHT FIELDS WITH MATTER https://doi.org/10.1070/QEL17618

Laser induced damage threshold and incubation effects of high-power laser system optics

S. Fourmaux, J.C. Kieffer

Abstract. **We present a laser induced damage threshold (LIDT) measurement technique where a mm-diameter non-Gaussian laser beam is used. This allows both a large number of measurements points and a large range of fluence to be sampled with a single measure. The method is used *in-situ*, inside the laser radiation–matter interaction vacuum vessel used for high power experiments with a 100 TW-class laser system. With our 2.5-Hz repetition rate laser system, the well-known incubation effect is observed where the laser damage threshold on the optics decreases with increasing number of laser shots. The incubation effect is studied with 22-fs laser pulses at a laser 2.5-Hz nominal repetition rate with several optics like dielectric mirrors and gold compression gratings irradiated by up to 9×10^3 laser shots.**

Keywords: *laser-induced damage of optics, high-power laser systems, incubation effects, fluence.*

1. Introduction

High power laser systems with ultrashort pulses are widely used to study laser-based acceleration of electrons and ions [1, 2], laser-induced X-ray and gamma emission [3], and warm dense matter production [4]. The advent of commercially available laser systems in the 100 TW up to the 10 PW range combined with a pulse duration around 20–50 fs opens the path for applications like X-ray and gamma imaging [5], as well as proton and X-ray fluorescence for material characterisation [6]. For academic studies, such laser systems are usually operated in the single laser shot regime in order to fully characterise laser radiation–matter interaction processes. For applications requiring a large number of shots in order to improve the signal-to-noise ratio within a reasonable time or to produce radiation or a particle dose, the laser system must be used both at its nominal peak power and repetition rate (usually 1–10 Hz for high energy systems). This raises the question of the laser system sustainability and design in order to operate safely in this regime. Normally, the operating fluence on the optical components should be chosen in order to work below their damage threshold with a safety factor, in case over-intensities occur during beam transport and manipulation. The most critical part of the optical system is after the compression stage where diameters of optical elements are large (10 cm diameter and more), while the femtosecond pulse duration is short. System designers would like to use the smallest diameter optics to reduce cost and space requirement while keeping the fluence in a safe range for the optics. One key component where this compromise between optics dimension and incident fluence must be achieved is, in double pass compressor configuration, the last compression grating as the highest intensities are produced at its output.

When laser light is incident on a material, photons are absorbed and the material starts to be ionised above some fluence threshold. Then, electrons are excited by impact ionisation, which leads to an avalanche effect until the produced free electrons plasma reaches the critical density where the laser energy is strongly absorbed. This critical electron density is associated with the laser induced damage threshold (LIDT) in ultrashort pulses less than 10 ps. In metals the material linear absorption is high enough to produce this excitation [7]. In transparent materials nonlinear absorption processes related to photoionisation like multi-photon ionisation or tunnelling ionisation must be considered. Heat transfer then occurs, producing liquefaction or phase change inside the material [8]. For longer laser pulses the laser pulse energy is absorbed by electrons and the energy is transferred to the lattice. Damage is associated with the transferred heat when it is high enough to melt, boil or fracture the material.

For dielectrics and long laser pulse, electrons originate mainly from the background carriers found in material impurities and defects, this is why laser damage threshold in this case is related to the material surface optical quality. For laser short pulses below 10 ps, the electrons produced by photoionisation in dielectrics are higher than the background electrons and the laser damage threshold is related to the material itself, this is why in this regime the damage process is said to be deterministic. Moreover, for short laser pulses the laser energy is deposited before any heat transfer to the lattice occurs [9, 10]. The interplay between each process can be complex and numerous studies have been made over the years due to their importance for high-power laser development or laser machining applications.

Several techniques have been used to measure the LIDT. In the statistical approach (S-on-1), the laser fluence is gradually incremented and it is observed if any damage occurs or not with a specific number of laser shots at the same position. Typically, the laser is focused down to a diameter of few tens of microns on the test optics. The same fluence is used several times on a fresh location far away from previous laser shots, which allows one to plot the damage occurrence probability versus the laser fluence [11]. In the diameter regression tech-

S. Fourmaux, J.C. Kieffer Institut National de la Recherche Scientifique Énergie, Matériaux et Télécommunications (INRS-EMT), Université du Québec, 1650 Lionel Boulet, Varennes J3X 1S2, Québec, Canada; e-mail: fourmaux@emt.inrs.ca

Received 8 July 2021
Kvantovaya Elektronika **51** (9) 751–758 (2021)
Submitted in English

nique, the damage area on a material is measured versus the laser fluence [12], and in the volume regression technique, the ablated material volume is measured versus the laser fluence [13]. It was also shown that techniques using a larger measurement area like the raster scan method are more sensitive to coating weaker areas as obviously the scanned area is larger [14]. Velpula et al. [14] reported a 33% decrease of the LIDT compared to a standard S-on-1 method. Apart from these mains techniques, many variations have been proposed. As an example, a single shot method based on the use of a Gaussian beam can also make it possible to correlate the fluence distribution with the damage morphology [15]. The variety of techniques can be coupled with several *in-situ* investigation procedures (time of flight, light scattering, plasma radiation measurement) or *ex-situ* investigation procedures where the damage study can be achieved with optical microscopy, AFM, STM, or mechanical profilometry. The large number of measurements reported in the literature can be related to the large number of laser damage threshold values. Some measurements are more sensitive to LIDT, other to the laser ablation threshold. For example, the statistical technique coupled with *ex-situ* damage observation is more sensitive to LIDT [16].

High peak power laser systems (100 TW and more) are operated under vacuum at the compression stage until the final use of target to avoid beam distortion during propagation. To this end, a primary vacuum is good enough but secondary vacuum without oil contaminants is often used with high repetition rate high power laser systems to lower organic contamination on optical surfaces. The laser damage threshold can vary with pressure depending on the material. The optics material fabrication and coating process influences its porosity and ability to trap water vapour or organic contaminants. Thus, it is preferable to determine the laser damage *in-situ* at the pressure of operation and with the same gaseous contaminants. For example, Nguyen et al. [17] studied LIDT in hafnia films and bulk fused silica. They reported for hafnia film a LIDT decrease by up to one order of magnitude for multiple pulses irradiation and pressure below 0.1 Torr. This behaviour was not observed on bulk silica and was attributed to oxygen deficiency in hafnia films [17].

It is well known that the LIDT changes as a function of the laser shot number done at the same place on a material [18]. This effect, called incubation, seems to be universal and has been observed in dielectrics, metals, semi-conductors and polymers. In optical components, this effect is present with bulk and multilayer materials. It has first been reported with a low repetition rate laser system in the range of 10 Hz [18–20]. More generally, the incubation effect is observed with high repetition rate systems from a few 100 Hz to MHz [20–26]. The LIDT value, ϕ_N, after N laser shots at the same position decreases as the number of shots N increases, reaching some stable value ϕ_∞ after some large number of shots. LIDT can be described by a simple law which is given by:

$$\phi_N = \phi_\infty + (\phi_1 - \phi_\infty) N^{S-1}, \quad (1)$$

where ϕ_1 is LIDT measured for one laser shot, and S is the so-called incubation factor [23]. The number of laser shots to get close to ϕ_∞ within 10% is typically found to be around 10000 laser shots [24]. The ϕ_∞ and S factor parameters change with material. The quantity ϕ_∞ depends on the pulse duration and laser repetition rate. For example, ϕ_∞ is measured to be around 38% of ϕ_1 for a stainless steel sample, 650-fs laser pulse duration and 100-kHz repetition rate [23]. The incubation factor is usually found, for short pulses, around 0.8–0.9 for metallic and dielectric samples (the incubation factor definition used in each work is not always the same) [20, 25]. It has been proposed that this behaviour is due to the thermal stress induced in the material or by the material surface roughening.

In this paper we present a LIDT measurement technique where a mm-diameter non-Gaussian laser beam is used. This allows one to sample from a single measurement both a large number of measurements points and a large range of fluence. We detail this method implementation inside the laser radiation–matter interaction vacuum vessel used for high power experiments with a 100-TW-class laser system. This way we have the same vacuum and organic contamination compared to our standard experimental conditions. We study the incubation effect with 22-fs laser pulses at a laser 2.5-Hz nominal repetition rate with several optics like dielectric mirrors and gold compression gratings. We show as expected that the laser damage threshold on the optics is lower when the laser shot number increases.

2. Experimental setup and LIDT measurement method

The measurements have been performed at the Advanced Laser Light Source (ALLS) facility at INRS-EMT, using a high-power Ti:sapphire laser. This laser system, located inside a radiation-protected area, can deliver on target as much as 175 TW (3.8 J, 22 fs, at a 2.5-Hz repetition rate). However, in these experimental series, in order to measure LIDT, we do not use the final amplification stage, which results in a maximum energy of 100 mJ on the test optics with a 22-fs laser pulse. At this energy level, the pulse-to-pulse stability measured over 1000 laser shots is 2% rms. We can estimate that a similar error will be made on the LIDT value determination and contribute to the total error.

The experimental setup is shown in Fig. 1a. The laser pulse is inserted into a vacuum vessel where it is focused using a 1.5-m focal length off-axis parabola. The experimental pressure is 8.5×10^{-5} Torr. After the focus position, the laser pulse is directed toward an imaging system to measure with a CCD camera the energy spatial distribution before the parabola focus at the test optics position where the laser spot size pupil is close to 10 mm diameter (around 15 cm distance away before the focus). A control imaging system is used to image the test optics position and insure that it is properly inserted and aligned in the laser beam path at the position where we image the laser beam.

A laser pulse cross section at the test optics position is shown in Fig. 1b; the pupil size is 7.5×9.2 mm. A large measurement area allows one to account for coating defects and impurities that could be missed by using a small measurement area and necessitates a high number of measurements positions. The near field has a top hat shape. Each pixel size in the test optics plane corresponds to 8.2 μm and the laser beam fluence is measured over 920000 pixels, each of them corresponding to a local fluence. Figure 1c shows the local fluence for each pixel position corresponding to the horizontal and vertical lines for the laser near field from Fig. 1b. The corresponding fluence histogram $H(f)$ is shown in Fig. 2 as a function of the calculated laser local fluence f for each pixel position at the test optics position. The laser fluence is deduced from the laser incoming total energy and the pixel size in the

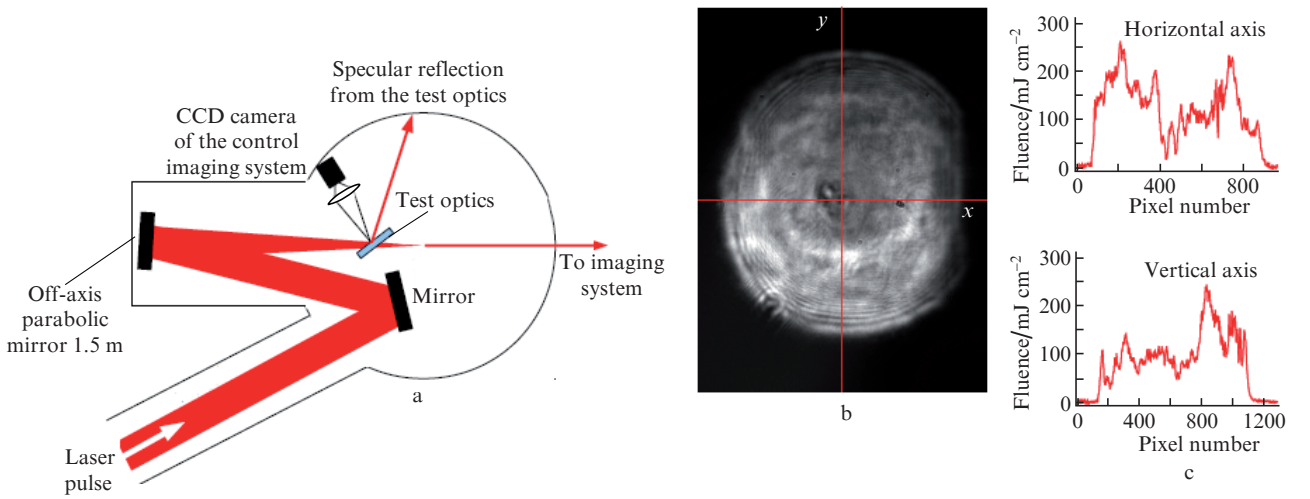

Figure 1. (Colour online) (a) Experimental setup; (b) laser pulse near field with a size of 7.5 × 9.2 mm used for LIDT measurements, and (c) fluence as a function of the pixel position corresponding to the horizontal and vertical lines shown on the previous image (b) by red lines.

test optics plane. For the calculation purpose, we assume a 51° incidence angle similar to the one found on gratings used in our pulse compressor. The right vertical axis in Fig. 2 shows $A(f)$ – the accumulated percentage of pixels in the laser near field with fluence higher than f, determined by the expression $A(f) = 100\sum_{i=0}^{f} H(i)/\sum_{i=0}^{f\max} H(i)$ (here, $f_{\max}$ is the maximum fluence obtained in the histogram). The average fluence $\sum_{i=0}^{f\max} iH(i)/\sum_{i=0}^{f\max} H(i)$ is 42 mJ cm^{-2}, and f spans from a few mJ cm^{-2} up to 280 mJ cm^{-2}.

We take advantage of the large fluence range measured in the laser pulse near field to avoid scanning energy and repeating the measurement to determine LIDT. For every single laser shot we can in principle image the resulting damage and rely each damaged position on the optics to the incoming fluence by the knowledge of the near field fluence distribution. In practice, this is difficult and time consuming to achieve precisely the superposition of the laser near field with the laser pulse imprint on the optics. The correspondence from the near field image with the damage imprint on the test optics is complex due to the use of different imaging systems with their own magnification in each case.

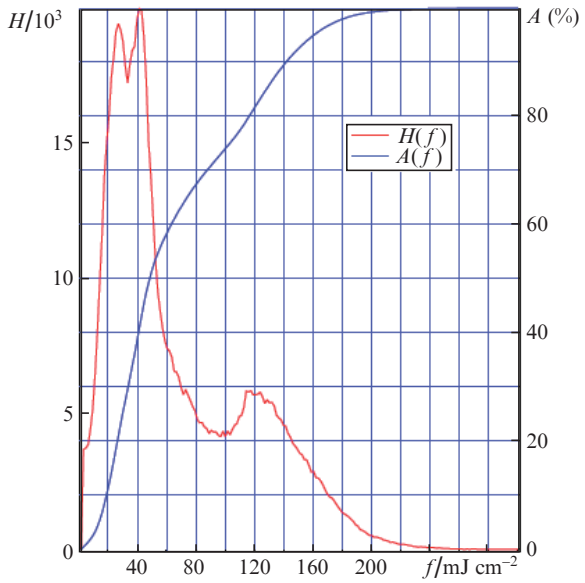

Figure 2. (Colour online) Laser pulse near field fluence histogram $H(f)$ where f is the laser pulse fluence at the test optics position (left axis) and laser pulse near field accumulated number of occurrences $A(f)$ (right axis). The $A(f)$ is also equivalent to the damaged area percentage as a function of the fluence.

We choose to use another approach: it is easier to determine inside the laser imprint on the test optics what percentage of the total area or of the total number of pixels have been damaged. We can reasonably assume that the damage is caused by the highest fluences present inside the laser near field. Thus, the damaged area percentage on the test optics corresponds to the same percentage value of pixels with the highest fluence in the laser near field image. Thus, assuming this hypothesis is correct, we can directly transpose $A(f)$ in term of the damaged area. For example, assuming that 50% of the laser imprint is damaged, we can see on the right vertical axis of Fig. 2 that it corresponds to a LIDT of 47 mJ cm^{-2}.

One advantage of this method is that a large number of fluences are obtained in only one single shot. The laser near field is measured inside an ellipse with typically 1054 × 1113 pixels (vertical and horizontal axes, respectively), which results in 921352 different fluence points. To measure the damaged area, the test optics surface could be imaged at a different angle and a wavelength to increase the light scattering and observe smaller damages. We choose to image the damaged area by directly imaging the test optics surface by illuminating it with collimated 800-nm laser light emitted from a fibre source at a nominal working angle of the optics. The surface is then imaged along the specular reflection of the incident light with a 25-mm objective. Typically, with this imaging system, the damaged surface corresponds to a laser imprint embedded inside an ellipse of 900 × 700 pixels ($y \times x$) which corresponds to 494801 measurement pixels.

A first example of measured images is presented in Figs 3a–3c for a multilayer dielectric coating deposited onto a glass substrate with respectively 1, 10 and 100 accumulated laser shots incident onto the test optics. The dielectric mirror manufactured by Altechna is a high reflectivity mirror designed for 750–850-nm bandwidth in p polarisation. The incidence angle is 20.55°. In this case the damage is initially

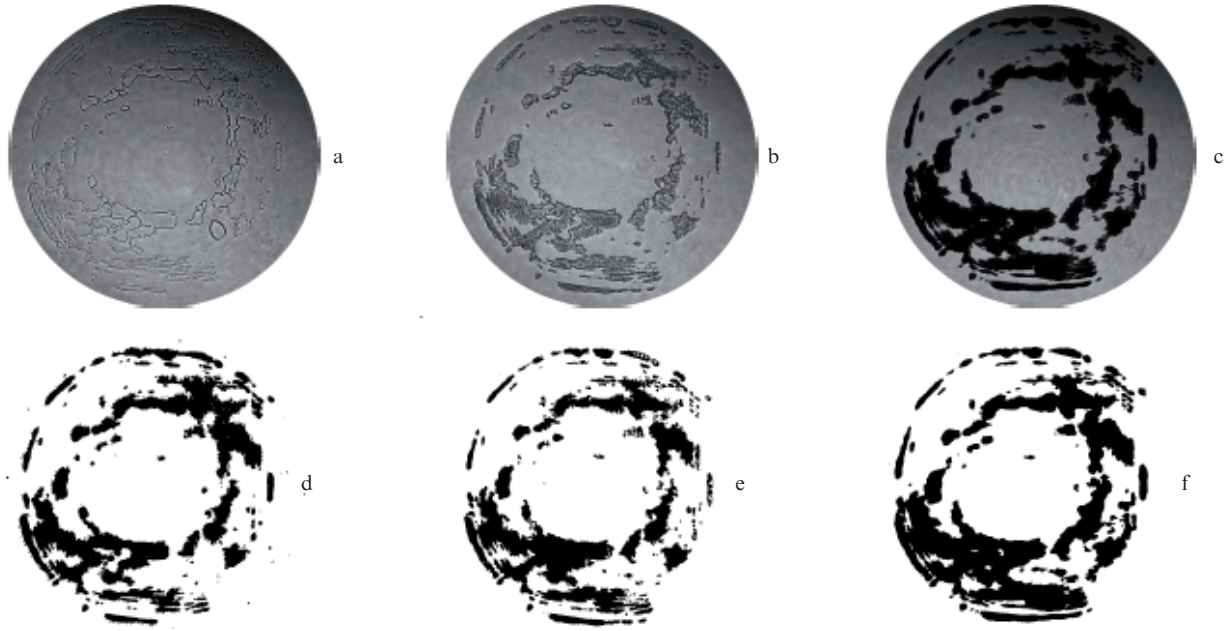

Figure 3. High reflectivity mirror (test optics) with a dielectric coating after the action of (a, d) 1, (b, e) 10 and (c, f) 100 laser shots: raw images of damages after the test optics is imaged with (a–c) 800-nm light and (e–f) images of the damages areas (shown by black colour) after an analysis. Only the analysed part corresponding to the incoming laser beam is shown for clarity.

related to the removal of some dielectric layers. After one laser shot only the fringes corresponding to the edges embedding the areas where the dielectric layers have been removed can clearly be seen as the reflectivity change is limited. After 10 laser shots a decrease in reflectivity can be associated with the removal of the dielectric layers. After 100 laser shots a complete loss of reflectivity can be observed suggesting a complete removal of the dielectric coating. A second example of measured images is shown in Figs 4a–4c for a gold grating where the gold is directly deposited onto a glass substrate with respectively 100, 1000 and 9000 accumulated laser shots incident onto the test optics with a 2.5-Hz repetition rate. The compression grating is ruled at 1480 lines per mm and designed for 800-nm, p-polarised light [manufactured by Plymouth Grating Laboratory (PGL)]. The incidence angle is 51.2° and the diffracted angle is 27.3°. In this case the damage is clearly related to a reflectivity loss due to the removal of the gold layer.

To find the area of the damaged surface, we determine the edges from the damaged area and integrate the corresponding surface in order to be able to count any pixels with small reflectivity variation which could occurs for example with a dielectric coating where only a few layers can be removed by an incident laser pulse. For each image on the test optics we

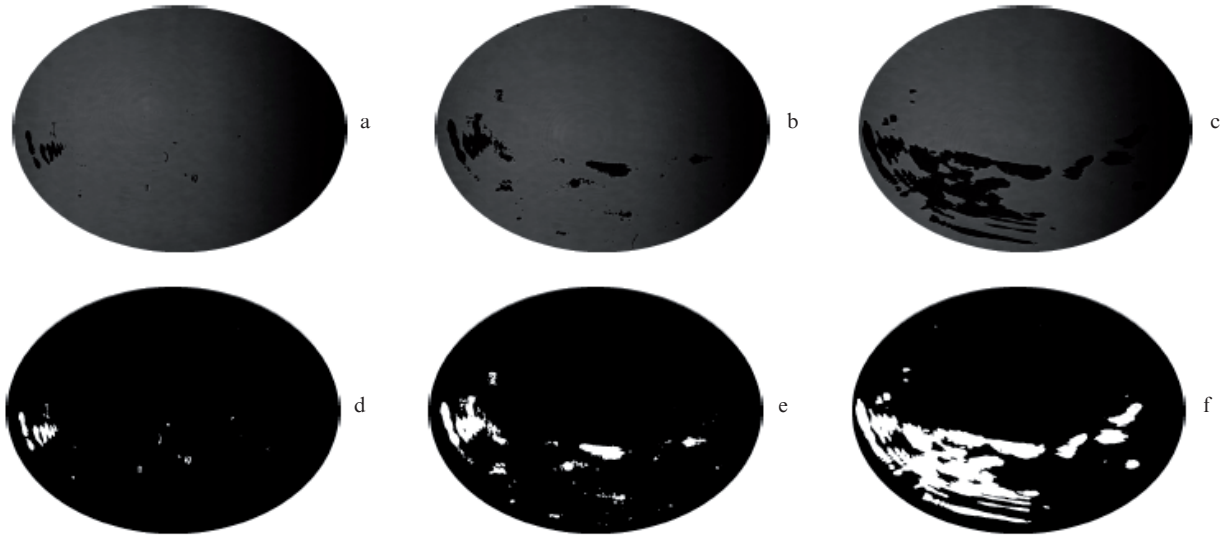

Figure 4. Tested gold grating after the action of (a, d) 100, (b, e) 1000, and (d, f) 9000 laser shots: raw images of damages after the test optics is imaged with (a–c) 800-nm light and (e–f) images of the damages areas (shown by white colour) after an analysis. Only the analysed part corresponding to the incoming laser beam is shown for clarity.

systemically follow the same procedure: 1. As image illumination might not be uniform, we flatten the background by fitting it with a 2 dimensional second order polynomial; 2. We subtract a fixed integer value (typically around 10 for a 8 bits image) from the image in order to set to zero the damaged area contour; 3. We invert the image and subtract a fixed integer value (typically around 250 for a 8 bits image) to set the undamaged contour to zero; 4. We fill the laser perimeter imprint that corresponds to the damaged surface with a specific colour and integrate the corresponding number of pixels. During the process, patterns that obviously correspond to artifacts due to dust in the imaging system or on the optical surface can be erased manually if required. The resulting analysed images are shown for the dielectric mirror in Figs 3d–3f where the starting image corresponds to respectively Figs 3a–3c.The resulting analysed images are shown for the gold grating in Figs 4d–f where the starting image corresponds to respectively Figs 4a–4c. LIDT measured by this method is related to some reflectivity change at the working wavelength or some obvious removal of material. We are not sensitive to any ablated precursors.

3. Results and discussion

We can clearly see qualitatively from Figs 3 and 4 the damage progress and the related affected surface increase for a higher number of laser shots.

The LIDT value as a function of the number of laser shots for the Altechna mirror optics is shown in Fig. 5a. The parameters corresponding to the fit for the incubation effect by Eqn (1) are $\phi_\infty = 108.5$ mJ cm^{-2}, $\phi_1 = 178.2$ mJ cm^{-2}, and $S = 0.78$. The incubation factor is close to the expected range. We found one test report from Altechna for a high reflectivity mirrors coating similar to the one we use where LIDT is measured in air with the S-on-1 method for a 50-fs laser pulse, 750–850 nm bandwidth, s polarisation, 45° incidence angle, and 1-kHz repetition rate [27]. The laser focal spot used for it is 150 μm. It was found that for a single shot LIDT is 600 mJ cm^{-2} and for 1000 laser shots LIDT is 320 mJ cm^{-2}. The use of s polarisation with 50-fs laser pulse duration is clearly less demanding than p polarisation with 22-fs laser pulse duration. Our results seem reasonable when we consider this reference.

The LDT value as a function of the number of laser shots for the PGL grating optics is shown in Fig. 5b. Note that for one laser shot no damage is seen on the test optics surface and the corresponding LIDT value is deduced to be above 280 mJ cm^{-2}. To obtain a more precise measurement, we should increase the energy to reach a higher energy fluence, but this would mean to start the power amplification stage, which results in a change of the near field and beam divergence. Another option is to work closer to the laser focal spot, but this changes completely the experimental calibration. The parameters corresponding to the fit for the incubation effect by Eqn (1) are $\phi_\infty = 115.3$ mJ cm^{-2}, $\phi_1 = 406.6$ mJ cm^{-2}, and $S = 0.67$. Poole et al. [28] measured the single shot laser damage threshold under vacuum to be 660 mJ cm^{-2} for conformal Au grating with 1480 lines per mm similar to our test optics with a 30-fs laser pulse duration [28]. The beam waist size at the focal spot used for the measurement is below 40 μm. Poole et al. also report for 1000 laser shot accumulation a 20% decrease of LDT corresponding to 528 mJ cm^{-2} that is a lot higher than ϕ_∞ measured to be 115.3 mJ cm^{-2} in our work. The relative low number of accumulated laser shots, longer pulse duration and small focal spot size used in this reference could explain the difference with our results.

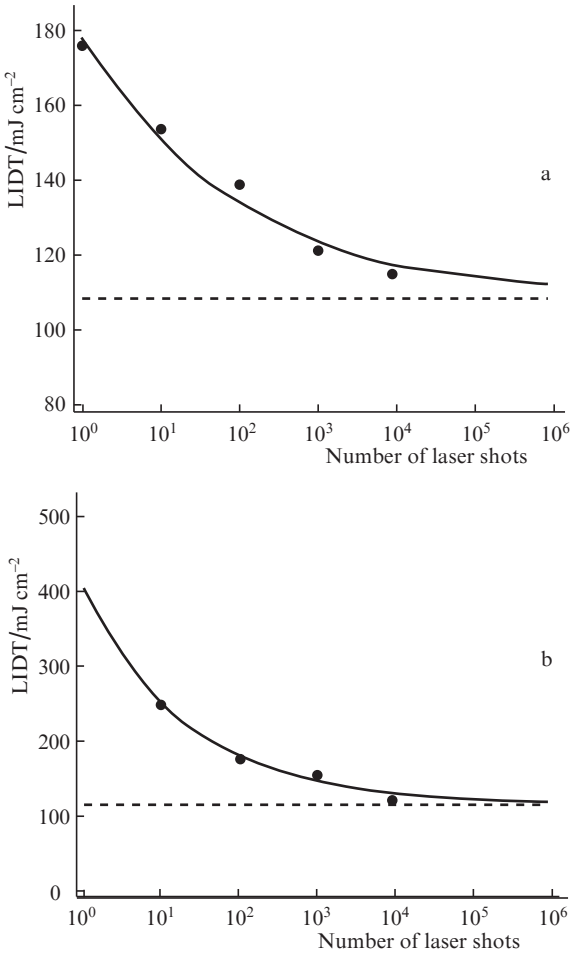

Figure 5. LIDT as a function of the number of laser shots at a pulse duration of 22 fs for (a) a high reflectivity mirror at 800 nm and for (b) a gold grating. The fit corresponding to Eqn (1) is also shown with the solid line. The dotted line indicates the value of ϕ_∞.

As a synthesis, Table 1 lists the incubation parameters ϕ_1, ϕ_∞ and S for various optics, obtained using the simple model [Eqn (1)]. This first parameter is the one of interest when designing a laser system. The first tested optics from Table 1 is the Altechna mirror. The second optics is the PGL grating. The third optics from Table 1 is a compression grating manufactured by Jobin Yvon (JY) in 2005. The gold is deposited on a resin layer fixed on a glass substrate. This compression grating is ruled at 1480 lines per mm and designed for 800-nm, p-polarised light with an incidence angle of 51.2° and a diffracted angle of 27.3°. Note again, that for one laser shot no damage is seen on the test optics surface and the corresponding LDT value is above 280 mJ cm^{-2}. The fourth optics from

Table 1. Incubation parameters found from the fit by Eqn (1) for various optics.

Tested optics	ϕ_1/mJ cm^{-2}	ϕ_∞/mJ cm^{-2}	S factor
Altechna mirror	178.2	108.5	0.78
PGL grating	406.6	115.3	0.67
JY grating	617.9	104.3	0.71
OS mirror	127.6	77.2	0.74

Table 1 is a large bandwidth dielectric mirror manufactured by OptoSigma (OS). This is a high reflectivity mirror designed for 700–900-nm, p-polarised light with an incidence angle of 20.55°. For all optics (except the Altechna mirror), the S factor values corresponding to the incubation equation (1) are below the expected interval range. This is still a simple model and more sophisticated study could be achieved that are outside the scope of this manuscript [24]. We note that for 9000 accumulated laser shots the measured value for LIDT is found to be close to ϕ_∞ as can be seen on Fig. 5, and so the value found for 9000 accumulated laser shots can be taken as a first approximation. LIDT for both gold gratings is measured to be higher than LIDT for dielectric mirrors. This is not what we would expect as dielectric coating are supposed to exhibit higher LIDT compared to metal coatings. However, LIDT depends on the coating fabrication process parameters: substrate material, coating process, cleaning procedures, and resulting coating stress. For example, for a dielectric coating designed for gratings, depending of the fabrication process and the residual stress, the resulting LIDT can be different by more than a factor of 4 [29].

There are some errors arising from the process of determining the damaged area in the LIDT determination process. A first error source is the positioning and size of the laser perimeter imprint ellipse on the test target. This can be estimated analytically if we consider the total number of pixels in the laser imprint to be P_{tot}, and a similar number P^+_{tot}, obtained as a result of an increase in the ellipse imprint by an amount p in percentage. We can write $P^+_{\text{tot}} = P_{\text{tot}}(1 + p/100)^2$ as the increase in pixels is related to the surface. The area difference in percentage will be $P_{\text{tot}}/P^+_{\text{tot}} - 1 = 1/(1 + p/100)^2 - 1$. This is correct if we assume that every extra pixel considered is undamaged. For example, if we assume that the error of the ellipse diameter measurement is 2.5 %, we obtain an area difference of 4.81 %. It results into an uncertainty around 3 % in fluence. Note that if an error occurs on the imprint size, a greater ellipse size compared to the correct one results in a lower damaged area percentage but it is counterbalanced by a lower fluence on each pixel and vice versa. At the end the effect is not important and the method is robust against error on the laser imprint size.

A second error source is the determination of the damaged area edges. The damaged edges resulting from the removal of the test optics material can be observed and appear as a black line more or less well defined depending of the optics working angle with the imaging system. It is difficult to know if the corresponding black pattern has to be counted as a damaged surface or not. The amount of the errors is proportional to the contour of the damaged surface. For every damaged area if we know P – the number of pixel inside it, we can define an average radius $r = \sqrt{P/\pi}$ in pixels and the corresponding perimeter $2\sqrt{\pi P}$ in pixels. If we assume that for a given damaged area percentage the error corresponds to the number of pixels in the perimeter, then we can easily plot the error as a function of the damaged area made during the area determination process. We plot this error E_e in Fig. 6, where we can see that it is higher for smaller surfaces and we can define a limit of a damaged area of 0.05 % below which it becomes unreasonable to use this method to measure LIDT.

We can now consider our laser system when it is operated at a nominal energy and check if the fluence used during operation is safe and optimal on the last compression grating and on the dielectric mirrors. The compression gratings are manufactured by Jobin-Yvon and the dielectrics mirrors by Altechna. The laser beam has to be transported from the compressor vessel to the interaction chamber located inside a radiation-protected area with 8 mirrors including the focusing optics. The transmission between the last compression grating and the target is 77 %. The last grating diffraction efficiency is 94 %. The nominal energy on target is 2.8 J (125 TW) but this can be increased up to 3.8 J (175 TW). The laser beam near field with a diameter of 95 × 86 mm at $1/e^2$ is shown in Fig. 7a. It is a super-Gaussian distribution different from Fig. 1b as the last amplification stage is operated, which changes the laser beam divergence and energy distribution. When we plot the laser beam profile, it can be fitted with a super-Gaussian on the order of ~7.7 as can be seen in Fig. 7b.

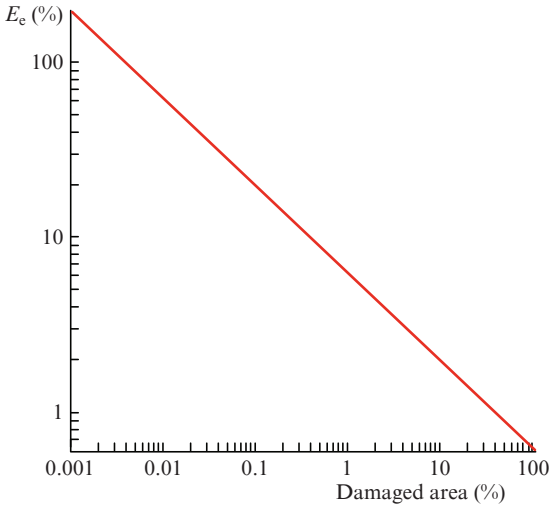

Figure 6. Error in determining the damaged area edges with the laser imprint on the test target.

Usually we calculate the fluence of the beam by assuming a top hat distribution with a beam diameter corresponding to the $1/e^2$ value. For example, with 2.8 J on the target the fluence on the off-axis parabola before the target is 42.7 mJ cm^{-2}. A more precise calculation consist in considering the fluence distribution F as

$$F = F_0 \int_0^{+\inf} r \exp[-2(r/R)^{7.7}] \mathrm{d}r\mathrm{d}\theta,$$

where r and θ are the radial and angular coordinates; F_0 is the peak fluence; and R is the beam radius at 1/e2. We obtain F_0 = 53.3 mJ cm^{-2}, which is 25 % higher compared to the previous value. More precisely, we can plot (Fig. 7c) the fluence histogram corresponding to the laser beam near field at a high power (corresponding to 2.8 J on the focusing optics). The corresponding median value is 45.9 mJ cm^{-2}, but we observe large fluctuations due to energy modulations that can be seen in the laser beam image. These fluctuations are ±38.1 mJ cm^{-2} in fluence and reaches a maximal fluence of 84 mJ cm^{-2}.

We can summarise in Table 2 the fluences obtained on the last compressor grating and on the first dielectric mirror (with 45° incidence) following the grating for the two energy settings. With an on-target energy of 2.8 J the safety factors are close to 1.4 both for the grating and the first mirror. With an on-target energy of 3.8 J the safety factors are slightly above 1 both for the grating and the first mirror. It means that for the highest energy there is no margin and any energy fluctuation

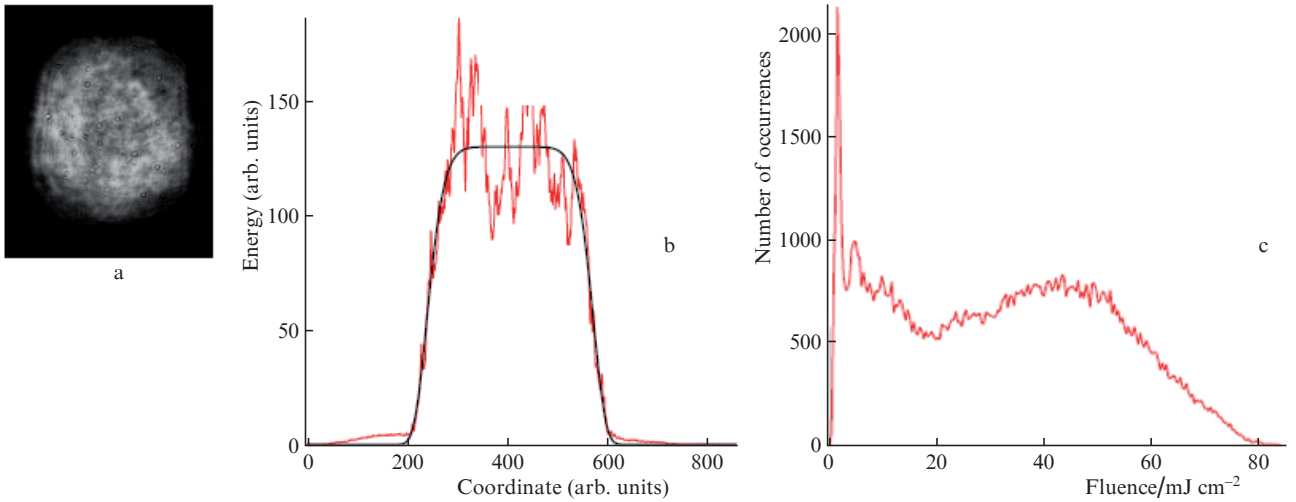

Figure 7. (a) Laser pulse near field on a target (energy of 2.8 J, and a beam size of 95 × 86 mm), (b) corresponding line profile where the super-Gaussian fit is indicated with a black continuous curve, (c) fluence histogram of the laser pulse near field on the off-axis parabola.

Table 2. Energy, average and maximum fluences on the surface of the last compression grating as well as the first mirror following the grating for two values of on-target energy.

E_{targ}/J	E_{grat}/J	F_{grat}^{av}/mJ cm^{-2}	F_{grat}^{max}/mJ cm^{-2}	E_{mir1}/J	F_{mir1}^{av}/mJ cm^{-2}	F_{mir1}^{max}/mJ cm^{-2}
2.8	3.82	37.3	73.5	3.64	40.1	78.9
3.8	5.18	50.6	99.6	4.94	54.4	107.1

could lead to a potential damage. Thus, it is safer to keep a maximum on-target energy of 2.8 J.

4. Conclusions

We presented a LIDT measurement technique where a mm-diameter non-Gaussian laser beam is used. This allows one to sample with a single measure both a large number of measurements points and a large range of fluence. This technique can be used *in-situ* with a high-power laser system to obtain the same vacuum environment where optics will be used. As expected, we observed incubation effects with the laser 2.5-Hz repetition rate. We measured a reduced LIDT for gold compression gratings and dielectric mirrors with laser pulses of 22-fs duration and 2.5-Hz nominal repetition rate. We show that it could be applied to our 100-TW high power laser system to define a safe energy operation of 2.8 J on the target.

Acknowledgements. We acknowledge our funding agencies: the Canadian Foundation for Innovation (CFI); le Ministere de l'Economie, de la Science et de l'Innovation from Quebec (MESI); the Natural Sciences and Engineering Research Council of Canada (NSERC); the Canada First Research Excellence Fund through the Plant Phenotyping Imaging Research Centre from the Global Institute for Food Security and University of Saskatchewan. We thank ALLS technical team: Guy Lebrun, Joel Maltais, Stephane Payeur, and Leonard Pelletier for the excellent support and help. We thank Plymouth Grating Laboratory and OptosSigma for providing test optical samples. We acknowledge Dr Steve MacLean for his financial support and help in providing optical samples.

The authors declare no conflicts of interest.

References

1. Lu W., Tzoufras M., Joshi C., Tsung F.S., Mori W.B., Vieira J., Fonseca R.A.,. Silva L.O. *Phys. Rev. ST Accel. Beams*, **10**, 061301 (2007).
2. Daido H., Nishiuchi M., Pirozhkov A.S. *Rep. Prog. Phys.*, **75** (5), 056401 (2012).
3. Kieffer J.C., Fourmaux S., Krol A. *Proc. SPIE Int. Soc. Opt. Eng.*, **10226**, 1022612 (2017).
4. Kieffer J.C. *FACETS*, **6**, 1390 (2021).
5. Döpp A., Hehn L., Götzfried J., Wenz J., Gilljohann M., Ding H., Schindler S., Pfeiffer F., Karsch S. *Optica*, **5** (2), 199 (2018).
6. Puyuelo-Valdes P., Vallières S., Salvadori M., Fourmaux S., Payeur S., Kieffer J.-C., Hannachi F., Antici P. *Sci. Rep.*, **11** (1), 9998 (2021).
7. Preuss S., Demchuk A., Stuke M. *Appl. Phys. A*, **61** (1), 33 (1995).
8. Stuart B.C., Feit M.D., Herman S., Rubenchik A.M., Shore B.W., Perry M.D. *Phys. Rev. B*, **53**, 1749 (1996).
9. Lenzner M., Krüger J., Sartania S., Cheng Z., Spielmann Ch., Mourou G., Kautek W., Krausz F. *Phys. Rev. Lett.*, **80**, 4076 (1998).
10. Tien A.-C., Backus S., Kapteyn H., Murnane M., Mourou G. *Phys. Rev. Lett.*, **82**, 3883 (1999).
11. Gallais L., Natoli J.-Y. *Appl. Opt.*, **42** (6), 960 (2003).
12. Elhadj S., Yoo J.H. *Opt. Lett.*, **42** (16), 3153 (2017).
13. Pietroy D., Maio Y.D., Moine B., Baubeau E., Audouard E. *Opt. Express,* **20** (28), 29900 (2012).
14. Velpula P.K., Kramer D., Rus B. *Coatings*, **10** (6), 603 (2020).
15. Sozet M., Neauport J., Lavastre E., Roquin N., Gallais L., Lamaignère L. *Opt. Lett.*, **41** (4), 804 (2016).
16. Sanner N., Utéza O., Bussiere B., Coustillier G., Leray A., Itina T., Sentis M. *Appl. Phys. A*, **94** (4), 889 (2009).
17. Nguyen D.N., Emmert L.A., Schwoebel P., Patel D., Menoni C.S., Shinn M., Rudolph W. *Opt. Express*, **19** (6), 5690 (2011).
18. Jee Y., Becker M.F., Walser R.M. *J. Opt. Soc. Am. B*, **5** (3), 648 (1988).
19. Rosenfeld A., Lorenz M., Stoian R., Ashkenasi D. *Appl. Phys. A*, **69** (1), S373 (1999).
20. Byskov-Nielsen J., Savolainen J.-M., Christensen M.S., Balling P. *Appl. Phys. A*, **101** (1), 97 (2010).

21. Rajeev P.P., Gertsvolf M., Simova E., Hnatovsky C., Taylor R.S., Bhardwaj V.R., Rayner D.M., Corkum P.B. *Phys. Rev. Lett*., **97**, 253001 (2006).
22. Machado L.M., Samad R.E., de Rossi W., Junior N.D.V. *Opt. Express*, **20** (4), 4114 (2012).
23. Niso F.D., Gaudiuso C., Sibillano T., Mezzapesa F.P., Ancona A., Lugarà P.M. *Opt. Express*, **22** (10), 12200 (2014).
24. Sun Z., Lenzner M., Rudolph W. *J. Appl. Phys*., **117** (7), 073102 (2015).
25. Nathala C.S.R., Ajami A., Husinsky W., Farooq B., Kudryashov S.I., Daskalova A., Bliznakova I., Assion A. *Appl. Phys. A*, **122** (2), 107 (2016).
26. Mustafa H., Pohl R., Bor T.C., Pathiraj B., Matthews D.T.A., Römer G.R.B.E. *Opt. Express*, **26** (14), 18664 (2018).
27. Plerpaitė V. https://www.altechna.com/wp-content/uploads/2018/10/hrsx750-850-aoi-45---0.32j-50.3fs-800nm-2015-10-08.pdf.
28. Poole P., Trendafilov S., Shvets G., Smith D., Chowdhury E. *Opt. Express*, **21** (22), 26341 (2013).
29. Smith D.J., McCullough M., Smith C., Mikami T., Jitsuno T. *Proc. SPIE Int. Soc. Opt. Eng*., **7132**, 7132QE (2008); https://doi.org/10.1117/12.817336.